THE JOURNAL OF PHYSICAL CHEMISTRY B

ARTICLE

pubs.acs.org/JPCB

Molecular Dynamics Simulation of Water Influence on Local Structure of Nanoconfined Polyamide-6,6

Hossein Eslami*,†,‡ and Florian Müller-Plathe‡

†Department of Chemistry, College of Sciences, Persian Gulf University, Boushehr 75168, Iran

‡Eduard-Zintl Institut für Anorganische und Physikalische Chemie and Center of Smart Interfaces, Technische Universität Darmstadt, Petersenstrasse 20, D-64287, Germany

ABSTRACT: Our recently developed molecular dynamics simulation method for simulating fluids confined in nanometric pores [Eslami et al. *J. Chem. Phys.* **2008**, *129*, 194702] is employed to simulate nanoconfined polyamide-6,6+water in contact with graphene monolayers. In this work, a number of dry and wet polymer samples, containing 3 and 6 wt % water at 350 K, confined in pores of different sizes as well as the bulk polymer samples are simulated. It is shown that both water and polymer molecules form organized layers beside the surfaces. The effect of nanoconfinement on the hydrogen bonding in the polymer+water system is studied in detail. It is shown that addition of water to the polymer replaces a fraction of looser amide−amide hydrogen bonds with amide−water ones. The distribution of hydrogen bond lengths shows that both the polymer and water form shorter length hydrogen bonds in the confined region compared to the bulk system. The number of hydrogen bonds between polymer and water molecules is shown to depend on the pore size and on the water content. In small pores, water molecules are forced by the surfaces into the polymer layers and form strong hydrogen bonds with the amide groups, a process that increases the water solubility of the polymer in small pores. Increasing the water content in larger pores increases the number of hydrogen bonds between water molecules and causes the formation of big clusters in the central region of the pore. In simulations of to 50 ns, it is shown that such big clusters grow with of time, and hence, phase separate out from the mixture.

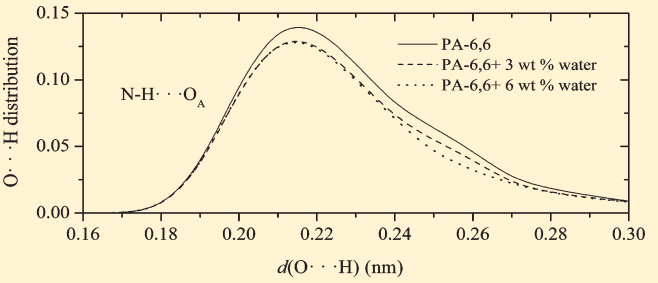

INTRODUCTION

The structure and dynamics of nanoconfined polymers in solutions is of prime importance in such applications as polymer enhanced-oil recovery,[1] gel-permeation and gel-electrophoresis,[2] size-exclusion and hydrodynamic chromatography,[3] drag reduction,[4,5] membrane separation,[6] and stabilization of colloidal dispersions.[7−9] Among the various polymers, polyamides (PAs) have important characteristics such as high thermal stabilities, good mechanical properties, excellent abrasion, low coefficient of friction, easy processing, and solvent resistance ,which makes them the most common engineering polymers applied to build machines in mechanical engineering.[10] Due to their excellent mechanical properties as well as their high selectivities, thin films of PAs are considered as high-performance materials with applications in the areas of reverse osmosis and nanofiltration membranes.[11] It is known that under high strain rates or low temperatures, the mechanical properties of PAs deteriorate, causing their embrittlement.[12] Plasticization with diluents such as water lowers the glass transition temperature of the polymer, which in turn, reduces the stiffness and the flow stress of the material and enhances the toughness and the strain to fracture.[13] The phenomenon of water plasticization in PAs is important, because of the existence of a large number of hydrophilic amide groups, which can hydrogen bond with the sorbed water molecules. Due to the importance of hydrogen bonding in PA-6,6, so far extensive experimental[14−18] and theoretical[19,20] research has been done on this subject. The results of these studies show that the macroscopic properties of PA-6,6 are strongly determined by the presence of the three-dimensional hydrogen bond network connecting the amide groups, which is responsible for the existence of different crystalline phases in the semicrystalline material.

From the experimental point of view, the advent of novel microscopy techniques such as surface force apparatus (SFA) and atomic force microscopy has enabled researchers to study the properties of nanoconfined thin films.[21,22] Recently, experimental measurements have been performed to elucidate the properties of complex nanoconfined systems.[23−29] In spite of considerable theoretical and experimental work, the properties of confined fluids are far from fully understood. This is due to the fact that the conventional continuum theories can not capture the properties at such small length scales. On the other hand, the experimental probing of such systems is difficult due to the small amount of material in the confined region. To date, most of the current information on the microscopic picture of the confined fluids comes from computer simulations.

Received: May 12, 2011
Revised: June 29, 2011
Published: July 08, 2011

Beginning with the early Monte Carlo (MC) simulation study of Snook and van Megen[30] and the molecular dynamics (MD) simulation of Cleveland et al.[31] on the confined Lennard-Jones (LJ) fluid between LJ surfaces, many simulations have been performed so far with the aim of shedding light on the structure and dynamics of more complex systems confined between surfaces. Following the molecular simulation strategies of simple LJ systems,[32−38] molecular simulations have been carried out some steps further to investigate properties of more realistic systems in confined geometries.[39−51] In this regard, many simulation reports on more complex systems such as the simulations of water confined between clay layers and graphite, alkanes confined between graphite and metal surfaces, and bead−spring or tangent hard-sphere chain models of polymers have been published in the literature.[39−51]

While, there exists a considerable number of simulation reports on the confined polymeric systems in the literature, two points are worth emphasizing: (1) In most of the simulations performed on confined polymer systems, the investigators used a generic bead−spring model to study, mostly, the equilibrium structure of the confined polymer melts. There are only a limited number of studies in which the investigators have tried to simulate realistic polymer chains in confinement. Examples of these are the recent works by Borodin et al.[52] on the MD simulation of the interface between poly(ethylene oxide) and TiO_2, by Daoulas et al.[53] and by Harmandaris et al.[54] on the united-atom MD simulations of thin polyethylene films supported by crystalline graphene, and by Eslami and Müller-Plathe[55,56] on the atomistic simulation of structure and dynamics of PA-6,6 oligomers in contact with graphite surfaces. (2) The type of experiments that the authors tried to mimic is often the SFA.[21,22] In the SFA, two solid surfaces are immersed in the fluid and the fluid in the confined region is in equilibrium with the bulk fluid. However, in most of the simulation reports in the literature, only the fluid in the confined region is simulated and it not kept in equilibrium with a bulk fluid. To be sure that the confined fluid is in equilibrium with the bulk fluid, the simulation must be performed in the grand canonical ensemble, which is just feasible for the case of simple LJ particles or very small molecules.[30,37] Due to very low probability for insertion or deletion of big polymer molecules, performing MC or MD simulations in the grand canonical ensemble is difficult. There is also a class of simulations in the literature in which the fluid in the confinement is simulated in connection with a reservoir of bulk molecules in the simulation box.[49,57] In such simulations it is believed that the fluid molecules in the confined region can be exchanged with bulk fluid molecules, and hence, the confined fluid can establish its equilibrium with the bulk fluid. The applicability of this method is also limited to small molecules, as the slow diffusion of the fluid in the confinement causes a very slow exchange rate.

Very recently we have developed a simulation method in which the fluid in the confined region is shown to be in equilibrium with the bulk fluid.[58] The results of this method are compared with the grand canonical ensemble MC simulation studies for LJ fluid[59−61] and with the MD simulation results of Choudhury and Pettitt[49] for water, in which the water confined between graphene sheets is simulated in the presence of bulk water molecules. The method has further been applied to investigate the structure and dynamics of PA-6,6 oligomers in contact with graphene surfaces.[55,56] As a continuation of our previous works,[55,56] in this work we aim to apply this method to propose a molecular-level understanding of local water−amide interactions and organizations, which allows us to study the effect of water on the layering, solvation force, free volume, hydrogen bonding, and clustering in nanoconfined PA-6,6+water films.

METHOD

In a confined fluid, in thermodynamic equilibrium with its surrounding bulk fluid, the measured force (or pressure) is expressed as a disjoining force (pressure), which is the difference between the force (pressure) in the confined region and that of the bulk fluid.[58] The properties of such nanoconfined systems are the subject of SFA experiments.[21,22] The statistical mechanical ensemble characterizing such a system is the grand canonical ensemble. Therefore, the simulation should ideally be done in the grand canonical ensemble. To overcome the difficulties with performing MD simulation in the grand canonical ensemble, especially for polymeric systems, we have recently formulated a new simulation scheme in which there is no need to connect the confined fluid to a reservoir of bulk molecules.[58] The method has been described elsewhere in detail.[58] Here we just give a brief explanation.

A system composed of a constant number of particles, N, confined between surfaces of constant surface area, A, at a constant temperature, T, and a constant parallel component of pressure, $P_{||}$, defined by eq 1, can be coupled to a thermostat and a barostat according to the algorithm described in ref 58. The parallel component of pressure is defined as

$$P_{||} = \frac{P_{xx} + P_{yy}}{2} = \frac{1}{3V}\sum_i m_i v_i^2 + \frac{1}{2V}\left[\sum_i \sum_{j>i} (X_{ij}\cdot F_{x,ij} + Y_{ij}\cdot F_{y,ij}) + \sum_i \sum_s (X_{is}\cdot F_{x,is} + Y_{is}\cdot F_{y,is})\right] \quad (1)$$

where P_{xx} and P_{yy} are the x- and y-components of pressure tensor, respectively, m is the atomic mass, v is the velocity, V is the volume, subscripts i and j show the atoms in the confined region, subscript s stands for the surface atoms, X and Y are the distances between particles in the x and y directions, respectively, and F_x and F_y are their corresponding forces. The parallel component of pressure is kept fixed by changing the distance between the confining surfaces.[58] This method is the extension of the original Berendsen et al.[62] method for coupling of a system to a thermostat and barostat. Therefore, the temperature is kept fixed by scaling the velocities at each time step according to the Berendsen[62] method. The coupling of the system to the barostat is taken place by changing the virial through scaling of interparticle distances in the z direction. This amounts to the scaling of the z-coordinates of all confined particles, and also surfaces to a scaling factor, λ, defined as[58]

$$\lambda = 1 - \beta\Delta t\frac{(P_{0,||} - P_{||})}{\tau_P} \quad (2)$$

where $P_{0||}$ is the target value of the parallel component of pressure (bulk pressure), β is the isothermal compressibility, Δt is the time step, and τ_P is the time constant for pressure coupling, determining the strength of coupling to the barostat. This method, which is called NAPT ensemble simulation hereafter, is shown to reproduce the results for confined LJ particles,[59−61] simulated in the grand canonical ensemble, and those for water confined between graphite surfaces,[49] simulated

dx.doi.org/10.1021/jp204423z |J. Phys. Chem. B 2011, 115, 9720–9731

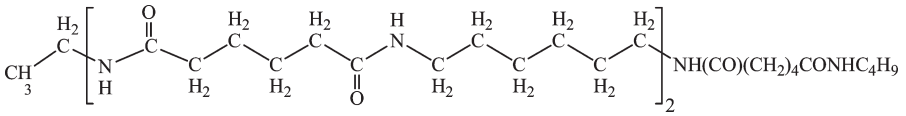

Figure 1. Chemical structure of PA-6,6 oligomers studied in this work.

in the presence of bulk water molecules. The method has further been applied to study structure and dynamics of confined PA-6,6 oligomers confined between graphite surfaces.[55,56] It is the purpose of this work to apply this method for the simulation of PA-6,6+water system nanoconfined between graphene surfaces.

SIMULATION DETAILS

In this work atomistic MD simulations have been performed for PA-6,6+water mixtures confined between graphene monolayers. Because of the sluggish dynamics of the polymer in confinement, short chains (trimers) of ethyl- and butyl-terminated PA-6,6, whose chemical structure is shown in Figure 1, were chosen for this purpose. The simulations were performed using our MD simulation package, YASP,[63,64] in the NAPT ensemble.[58] Here just the fluid in the confined region was mobile, and the graphene surfaces were kept stationary. The temperature was kept constant at 350 K, using a Berendsen[62] thermostat, and the parallel component of pressure was kept constant at 101.3 kPa, using the aforementioned simulation method in the NAPT ensemble.[58] The temperature and pressure coupling constants were 0.2 and 2.0 ps, respectively. The force field parameters for PA-6,6 as well as for the confining surfaces, graphene surfaces, are reported in our former publication.[55] For water, the extended simple point charge (SPC/E) model[65] was used. Nonbonded interactions were applied fully between atoms interacting through torsion terms (1−4 interactions). All nonbonded interactions were truncated at 0.95 nm with a reaction-field correction for the Coulombic interactions.[66] The reaction-field dielectric of PA-6,6+water mixtures was approximated as the sum of mass fractions of components multiplied by their corresponding reaction-field dielectrics; the reaction-field dielectric of PA-6,6 was taken to be 5.5,[19,67] and that of water was taken equal to 72.0.[68] The parameters for unlike interactions were determined using Lorentz−Berthelot mixing rules.[66] All bond lengths were constrained using the SHAKE algorithm.[69,70] An atomic Verlet neighbor list was used, which was updated every 15 time steps, and the neighbors were included if they were closer than 1.0 nm. The time step for the leapfrog integration scheme[66] was 2.0 fs.

The concentration of water in PA-6,6 was adopted according to our recent grand canonical ensemble simulation results for solubility of water in bulk PA-6,6 20-mers, which is 6 wt % water.[71] Because of the fact that the solubility of sorbents in shorter polymer chains is lower than the longer ones,[72] samples of PA-6,6 oligomers containing 3 wt % as well as 6 wt % water were prepared. While according to our previous calculations,[71] a bulk sample of PA-6,6 containing 6 wt % water is expected to phase separate into two phases, simulation of systems of such composition enables us to study the effect of confinement on the sorption ability of polymer. To prepare mixtures of water dissolved in polymer, water molecules were randomly inserted in the polymer matrix at 500 K. In fact, the inclusion of water has not been done at 350 K, in order not to preclude the formation of clusters due to the low diffusion coefficient of water in pores at 350 K. Inclusion of water molecules at 500 K enables water molecules to possibly travel the whole box size during the first few nanoseconds of simulation. Since the solubility of water in PA-6,6 is lower at higher temperatures,[71] we did a cluster analysis test at 500 K to be sure the water was not phase separated. The samples of PA-6,6+water then cooled out to 350 K at a rate of 15 K/ns. The higher solubility of water in PA-6,6 at lower temperatures excludes the freezing, in the cooling stage, of phase-separated structures formed at higher temperatures.

In this work, seven different confined PA-6,6+water systems as well as the bulk PA-6,6 were simulated. To study the water effect on the static and dynamic properties of polymer in confinement, seven similar dry samples, with about the same average intersurface separations as their corresponding wet samples, as well the bulk dry polymer were also simulated. The characteristics of the

Table 1. Description of Systems Simulated in This Work[a]

system	n_O	n_W	N_g	N	A (nm^2)	$\langle h \rangle$ (nm)
dry samples:						
S_1	80		4032	17344	105.62	1.097
S_2	93		4032	18852	93.98	1.287
S_3	89		3108	16540	71.22	1.473
S_4	85		2508	14876	63.67	1.709
S_5	95		2508	16036	51.65	1.861
S_6	106		1972	16240	31.33	2.450
S_7	107		1144	14700		4.135
S_8 (bulk)	150			17400		
wet samples:						
3 wt % water						
S_1^3	77	90	4032	17266	105.62	1.080
S_2^3	89	104	4032	18700	105.62	1.267
S_3^3	86	101	3108	16495	81.41	1.468
S_4^3	82	96	2508	14816	65.69	1.703
S_5^3	92	108	2508	16012	65.69	1.857
S_6^3	103	120	1972	16252	51.65	2.508
S_7^3	104	122	1144	14718	29.97	4.150
S_8^3 (bulk)	100	117		11951		
6 wt % water						
S_1^6	75	181	4032	17307	105.62	1.075
S_2^6	87	210	4032	18786	105.62	1.274
S_3^6	84	203	3108	16569	81.41	1.471
S_4^6	80	193	2508	14875	65.69	1.707
S_5^6	90	217	2508	16107	65.69	1.867
S_6^6	100	241	1972	16267	51.65	2.512
S_7^6	100	241	1144	14611	29.97	4.138
S_8^6 (bulk)	100	241		12323		

[a] n_O and n_W represent the number of oligomers and the number of water molecules, respectively. N_g and N stand for the number of C atoms per each graphene sheet and the total number of atoms, respectively. A is the surface area, and $\langle h \rangle$ is the average surface separation at T = 350 K and $P_\parallel$ = 101.3 kPa.

dx.doi.org/10.1021/jp204423z |J. Phys. Chem. B 2011, 115, 9720–9731

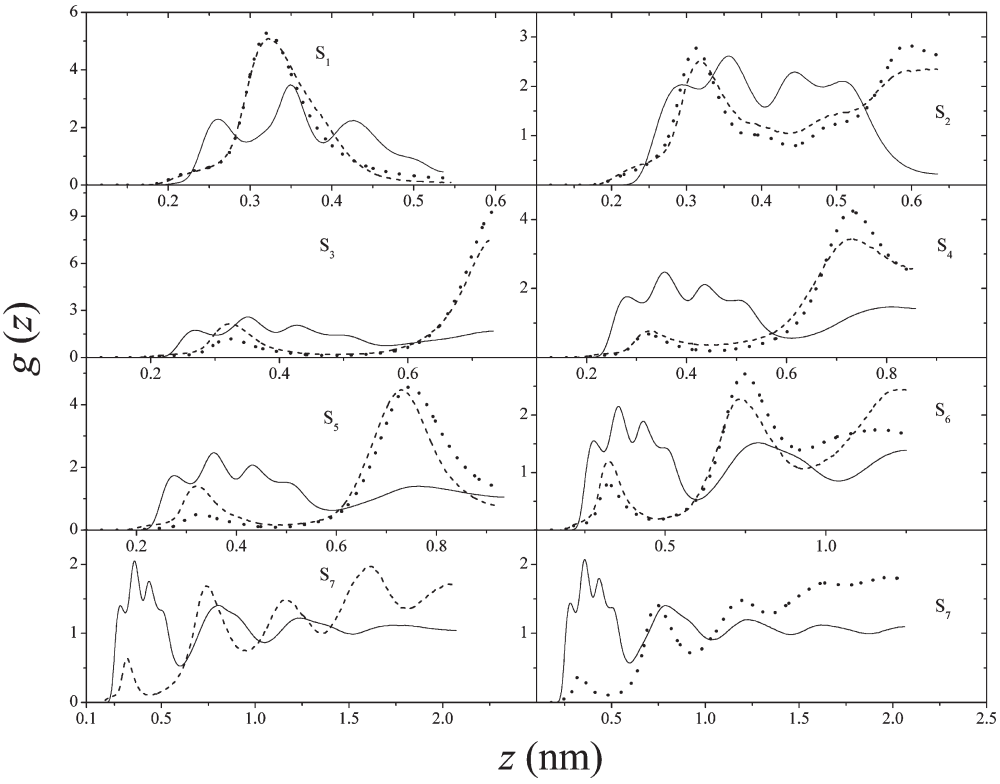

Figure 2. The surface-polymer (full curves) and surface-water distribution functions along the *z*-axis. Dashed and dotted curves represent the distribution functions for wet samples containing 3 and 6 wt % water, respectively. The distributions are cut off at half pore widths. The distribution functions for PA-6,6 oligomers do not show a considerable difference in dry and wet samples. Therefore, in this figure the surface-polymer distribution functions are plotted only for dry polymer samples.

studied systems are tabulated in Table 1. In all wet polymer samples, we tried to change the number of polymer and water molecules in such a way to have mixtures of fixed composition confined in pores of nearly the same widths as their corresponding dry samples. This provided us an opportunity to study the effect of added water on the structure of nanoconfined polymer, keeping fixed the effect due to the surfaces. Moreover, we have prepared mixtures confined in pores with a variety of widths to be able to study the effect of pore size on the structure of both dry and wet polymer samples. Following the cooling step, as explained above, the configurations at 350 K were subsequently simulated at a fixed temperature (350 K) and a fixed parallel component of pressure (1.013 kPa) for 10 ns. Unless otherwise stated, simulations were performed over another 10 ns time span for the sake of data collection.

RESULTS AND DISCUSSION

One-Dimensional Distribution Functions. It is known that fluids in confined geometries form layered structures near the surfaces. Figure 2 shows the surface-polymer and surface-water distribution functions along the *z*-axis. Because of the symmetry, the distribution functions are cut off at half of the pore widths, $\langle h \rangle$. The deviations of depicted profiles in Figure 2 from one show that both confined oligomers and water reveal characteristics different from the bulk fluid by forming layered structures near the surfaces. At small intersurface separations, around 1.0 nm, both polymer and water show one well-formed layer in the vicinity of each surface, with that of the polymer consisting of three bumps. Increasing the surface separation to about 1.3 nm, the bigger polymer molecules form one diffuse layer near each surface, while for smaller water molecules a new layer in the central region of the box is observed. Increasing the distance between the surfaces, water molecules show sharper distribution functions in the central polymers layers, compared to the polymer layers located in the vicinity of the surfaces. This might indicate that water is phase-separating out in the central region of the box, which will be clarified in the next sections. The results in Figure 2 further indicate that with changing the number of polymer/water molecules at constant composition, constant temperature, and constant bulk pressure, the number of layered structures for both polymer and water changes, depending on the pore width. At surface separations around 4.0 nm, the surface—polymer distribution functions do not show distinct peaks at distances about 1.5 nm away from the surfaces, but for water molecules, pronounced peaks are seen even in the center of the box.

Solvation Force. The solvation force, f_s, is defined as the force acting on two solid surfaces immersed in a liquid, and is expressed in terms of pressure components as

$$\langle f_s \rangle = A(\langle P_\perp \rangle - \langle P_\parallel \rangle) \quad (4)$$

where A is the surface area and $P_\perp$ is the perpendicular component of pressure and brackets indicate the average. The average solvation forces as a function of average separation distances, for both wet and dry polymer samples, are shown in Figure 3. The results in Figure 3 show that both dry and wet polymer samples show nearly identical solvation forces at the

dx.doi.org/10.1021/jp204423z |J. Phys. Chem. B 2011, 115, 9720–9731

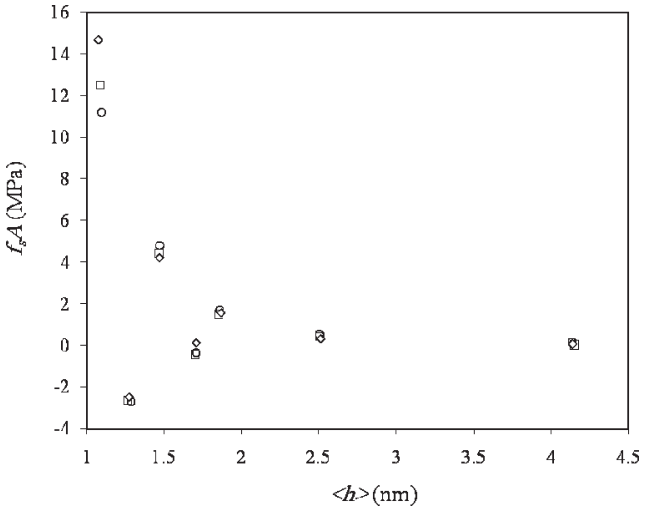

Figure 3. The solvation force as a function of surface separation at T = 350 K and $P_{||}$ = 101.3 kPa for dry PA-6,6 (○), PA-6,6 + 3 wt % water (□), and PA-6,6+ 6 wt % water (◇). The points represent the calculated average solvation forces as functions of average surface separations, $\langle h \rangle$, for systems tabulated in Table 1.

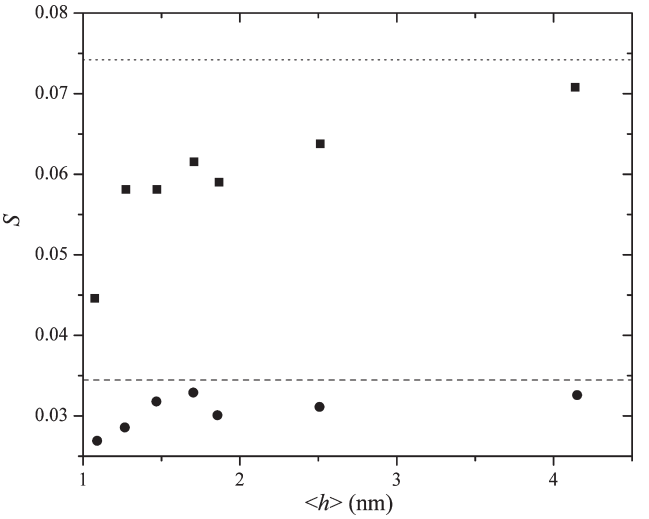

Figure 4. Swelling degrees as a function of average intersurface separation for PA-6,6 + 3 wt % water (●), and PA-6,6+ 6 wt % water (■). The dashed and dotted lines represent the corresponding bulk values, respectively.

same intersurface separations, with those of higher water contents staying a bit higher. The period of oscillations in the solvation force curves is equal to the period of formation/deformation of layered structures beside the surfaces. In fact well-formed layered structures with sharper density peaks correspond to more repulsive solvation forces, while the diffuse layers correspond to the negative solvation forces.[55,56,58] Therefore, the oscillation patterns in the solvation force curve correspond to the ordering/disordering of layers parallel to the surfaces.

Polymer Swelling. The change in volume of a polymer due to the sorption of a sorbant is usually referred to as the swelling degree. The knowledge of swelling behavior of polymers in the presence of dissolved species is of importance in the description of interactions between polymer-penetrant systems and in the practical applications addressed in the Introduction. The swelling degree, S, is defined as

$$S = \frac{V_{PA+W} - V_{PA}}{V_{PA}} \quad (5)$$

where V_{PA+W} and V_{PA} represent the molar volumes of PA-66 +water and that of PA-66, respectively, at the same intersurface separation. The effect of water sorption on the swelling degree of the polymer can be specified by knowing the volumes of mixture and pure polymer under the same conditions. The calculated swelling degrees are shown in Figure 4 as a function of surface separation. The results in Figure 4 show that sorption of water in PA-6,6 swells the polymer, and the amount of swelling depends on the intersurface separation; in smaller-size pores the polymer swells less. As there is no report in the literature on the swelling of nanometric PA-6,6 films, the results obtained in this section can not be compared with experiment. The macroscopic bulk sample, however, does not have swelling properties identical to the ultrathin samples. However, as an indication of agreement of our calculations with experiment, it is worth noting that our results for bulk samples (shown in Figure 4) are quite comparable with the experimental[73] swelling results at 300 K (0.03 and 0.06 for samples containing 3 and 6 wt % water).

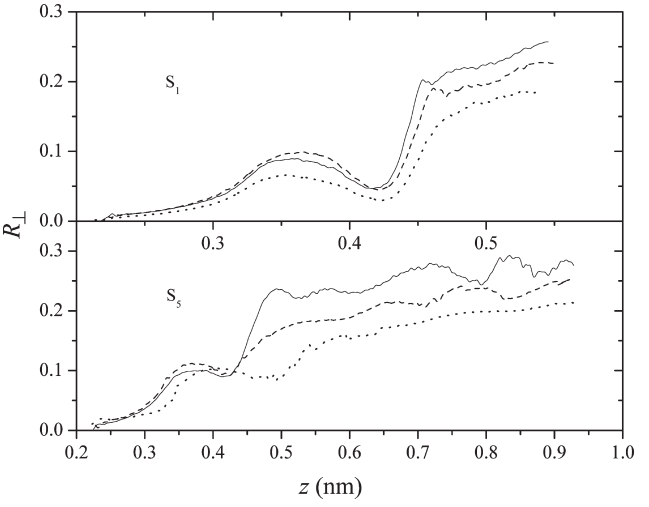

Figure 5. Normalized square perpendicular component of end-to-end vector for dry PA-6,6 (full curve), PA-6,6 + 3 wt % water (dashed curve), and PA-6,6+ 6 wt % water (dotted curve).

Chain Conformation. Particularly useful information on the structure of wet confined oligomers can be obtained by analyzing the end-to-end distance of dry and wet samples. If $\mathbf{r}_1$ and $\mathbf{r}_n$ denote the position vectors of the first and last atoms in the chain, respectively, the end-to-end vector is defined as $\mathbf{R} = \mathbf{r}_1 - \mathbf{r}_n$. In Figure 5 we have shown the normalized perpendicular component of the square end-to-end vectors, $R^2_\perp = (z_1 - z_n)^2/R^2$ for dry and wet polymer samples S_1 and S_5, as typical examples, as a function of surface separation. The results in Figure 5 show that polymer chains adopt a flattened confirmation beside the surfaces. With increasing the distance between the surfaces, the chain conformation in the intermediate region of the box gets close to the bulk-like behavior (random orientations). Our results also indicate that addition of water to the polymer matrix more extends the polymer chains parallel to the surfaces, with a smaller normalized z-component of the end-to-end vector. This

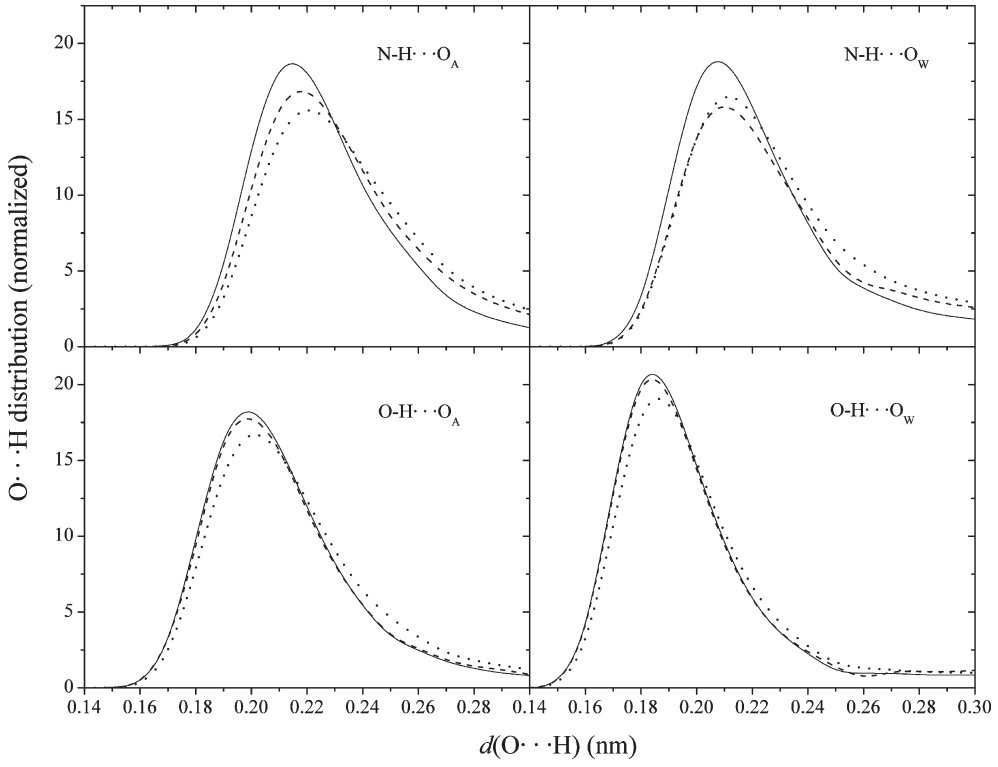

Figure 6. Normalized distribution functions for hydrogen bond lengths. The curves indicate the distribution functions for S_2^3 (solid curves), S_5^3 (dashed curves), and S_8^3 (dotted curves).

extension is more pronounced in the case of polymer samples containing 6 wt % water. The results are consistent with the results of the former section on the swelling of polymer in the presence of water.

Hydrogen Bonding. The hydrogen bonding in PA-6,6 is responsible for the formation of a three-dimensional network, influencing the mechanical properties of the polymer. The water−amide hydrogen bonding affects the macroscopic properties of PAs, such as the decrease in the main relaxation temperature and the density and free-volume variations of PAs as a function of water content. According to the two-step model of Starkweather,[73] in the bulk PA samples, the first water molecules form two hydrogen bonds between two pendent carbonyl groups belonging to different chains. At a concentration around one water molecule per two amide groups (about 7 wt %), this sorption mode saturates, and additional water molecules form clusters between carbonyl and NH groups. This leads to another saturation concentration, at about three water molecules per two amide groups (about 21 wt %), at room temperature. Since a significant number of amide groups are unavailable to water molecules, the water solubility of PA-6,6 at 300 K (about 10 wt %) is much lower than this saturation concentration. Although hydrogen bonding in bulk PA-6,6+water sample has been the subject of a number of experimental[14−18] and theoretical[19,20,55] reports, so far no report exists on the study of hydrogen bonding in confined wet PA-6,6. In this work, we aim to provide a quantitative description of water−amide hydrogen bonding in confined polymer samples.

Distribution of Hydrogen Bond Lengths. Here, the water−amide hydrogen-bonds are analyzed, considering (1) amide NH as the donor and amide O as the acceptor, N−H···O_A, (2) amide NH as the donor and water O as the acceptor, N−H···O_W, (3) water OH as the donor and amide O as the acceptor, O−H···O_A, and (4) water OH as the donor and water O as the acceptor, O−H···O_W. The results of previous studies of this group[19,20] show that including amide nitrogen as an acceptor results in nearly a very small increase in the number of hydrogen bonds; therefore, the amide nitrogen has not been taken into account as a hydrogen-bond acceptor in this work. The hydrogen bonds are defined according to a geometric criterion in which the distance between the hydrogen of the donor group and the acceptor has to be less than a limiting value, and the donor−hydrogen−acceptor angle has to be bigger than a limiting angle. In this work, the limiting angle is chosen to be 130°, according to the previous literature. To choose the limiting distance, we have shown in Figure 6 the hydrogen bond length distributions for systems S_2^3, S_5^3, and S_8^3 as typical examples. The results show that, on average, the longest and the shortest hydrogen bonds are due to the N−H···O_A and O−H···O_A, respectively. With decreasing the pore width, the maxima shift to smaller lengths. This means that the hydrogen bonds formed in narrower pores are stronger than the corresponding ones formed in wider pores (or in bulk). According to the results in Figure 6, we have chosen a limiting distance of 0.29 nm for taking into account a H···O bond as a hydrogen bond.

Water Effect on Hydrogen Bonding in Pore. The average number of hydrogen bonds per donor for all above-cited hydrogen bond types is tabulated in Table 2. According to the results tabulated in Table 2, the average number of N−H···O_A hydrogen bonds depends on the water content of the polymer and on the layering behavior of confined polymer between the surfaces. In highly confined systems, for example, in systems S_1, S_1^3, and S_1^6, geometrical restrictions hinder the formation of N−H···O_A hydrogen bonds. In systems S_2, S_2^3, and S_2^6, with minimum density of polymer in the confined region (see Table 1), polymer molecules form diffuse layers

dx.doi.org/10.1021/jp204423z |J. Phys. Chem. B 2011, 115, 9720–9731

Table 2. The Average Number of Hydrogen Bonds per Donor in Systems Simulated in This Work

	hydrogen bond type			
system	NH···O_A	NH···O_W	OH···O_A	OH···O_W
dry samples:				
S_1	0.54			
S_2	0.76			
S_3	0.68			
S_4	0.74			
S_5	0.73			
S_6	0.75			
S_7	0.76			
S_8 (bulk)	0.76			
wet samples:				
3 wt % water				
S_1^3	0.50	0.10	0.56	0.18
S_2^3	0.68	0.10	0.50	0.30
S_3^3	0.67	0.10	0.53	0.31
S_4^3	0.63	0.11	0.55	0.29
S_5^3	0.61	0.10	0.52	0.33
S_6^3	0.67	0.11	0.56	0.29
S_7^3	0.68	0.10	0.54	0.32
S_8^3 (bulk)	0.68	0.10	0.54	0.30
6 wt % water				
S_1^6	0.44	0.13	0.41	0.37
S_2^6	0.67	0.12	0.31	0.52
S_3^6	0.54	0.19	0.45	0.39
S_4^6	0.63	0.14	0.37	0.50
S_5^6	0.58	0.16	0.39	0.48
S_6^6	0.65	0.12	0.34	0.55
S_7^6	0.68	0.10	0.28	0.59
S_8^6 (bulk)	0.68	0.15	0.38	0.54

with negative solvation forces (see Figure 2). Therefore, in these systems the amide groups are located in lower density neighborhoods compared to the systems with well formed structures, and hence, are less hindered spatially. This enables them to better form hydrogen bonds. Increasing the distance between the confining surfaces decreases the number of hydrogen bonds due to the increase in the geometrical restrictions. At intersurface distances larger than about 2.5 nm the maximum number of hydrogen bonds is observed. This is in agreement with the results of our previous work on the hydrogen bonding in nanoconfined PA-6,6.[55] Addition of water to PA-6,6 oligomers reduces the number of N−H···O_A hydrogen bonds. According to the data in Table 2, around 10% −15% of the N−H···O_A hydrogen bonds are broken with the addition of 3 wt % water to the polymer. Such a reduction in the N−H···O_A hydrogen bonds is responsible for the decrease in the nanoconfined PA-6,6 densities (swelling). Addition of more water molecules to the system (up to 6 wt %) breaks very few additional N−H···O_A hydrogen bonds, which is in agreement with the dynamical mechanical analysis results of Le Huy and Rault[13] on PA samples at 300 K. Similar results have formerly been found on bulk polymers by Goudeau et al.[19] for PA-6,6, by Müller-Plathe[74] for poly(vinyl alcohol), and by Borodin et al.[75,76] for poly(ethylene oxide).

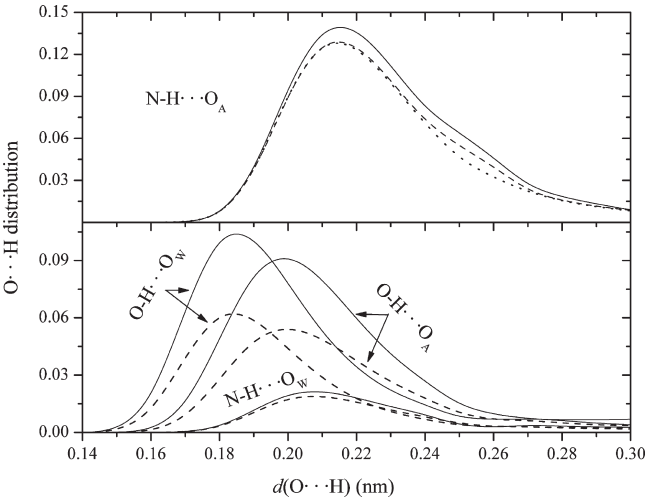

Figure 7. Distribution of hydrogen bond lengths in S_2. The hydrogen bond types are indicated in the figure. The curves in the top panel indicate the distribution functions for PA-6,6 (full curve), PA-6,6 + 3 wt % water (dashed curve), and PA-6,6+ 6 wt % water (dotted curve). In the bottom panel, the full and dashed curves belong to PA-6,6+water mixtures containing 6 and 3 wt % water, respectively.

The results in Table 2 further indicate that the number of N−H···O_W hydrogen bonds does not change considerably with the water content and with the intersurface distance. Comparison of the results in the second and third columns of Table 2 show that with the addition of water to PA-6,6, nearly the same number of N−H···O_A hydrogen bonds are replaced by N−H···O_W ones. To illustrate which fraction of N−H···O_A hydrogen bonds (from the point of view of hydrogen bond length) are replaced by N−H···O_W ones, we have shown in Figure 7 the composition dependence of the hydrogen bond length distributions in dry and wet S_2 systems, as typical examples. The results show that addition of water to the polymer breaks a fraction of looser N−H···O_A bonds (with longer bond lengths). As a result, water molecules have the chance to get close to such free NH groups, to form hydrogen bonds with.

According to the results in Table 2, the number of O−H···O_A hydrogen bonds also does not depend substantially on the pore width, but depends on the water content of polymer. A close look at the distribution functions in Figure 2 shows that water−amide hydrogen bonding can take place inside the organized polymer layers (among the water molecules located in polymer layers and their neighboring amide groups) and between the organized polymer layers (among the water molecules located between the polymer layers and the amide groups in the neighboring polymer layers). The magnitudes, however, depend on the intersurface separation, and hence, on the layering pattern of both polymer and water. For example, in system S_1^3 the surfaces force water molecules into the polymer layers. Therefore, water−amide hydrogen bonding takes place inside the organized polymer layers. On the other hand, in system S_2^3, in addition to the water molecules presenting in the polymer layer, a second layer of water molecules are seen in the center of pore. Here, both water molecules in the polymer layer and those presenting between the polymer layers are capable of hydrogen bond formation.

The fraction of amide groups that do not share hydrogen bonds with any water molecules is around 0.70 and 0.55 in the case of PA-6,6 samples containing 3 and 6 wt % water,

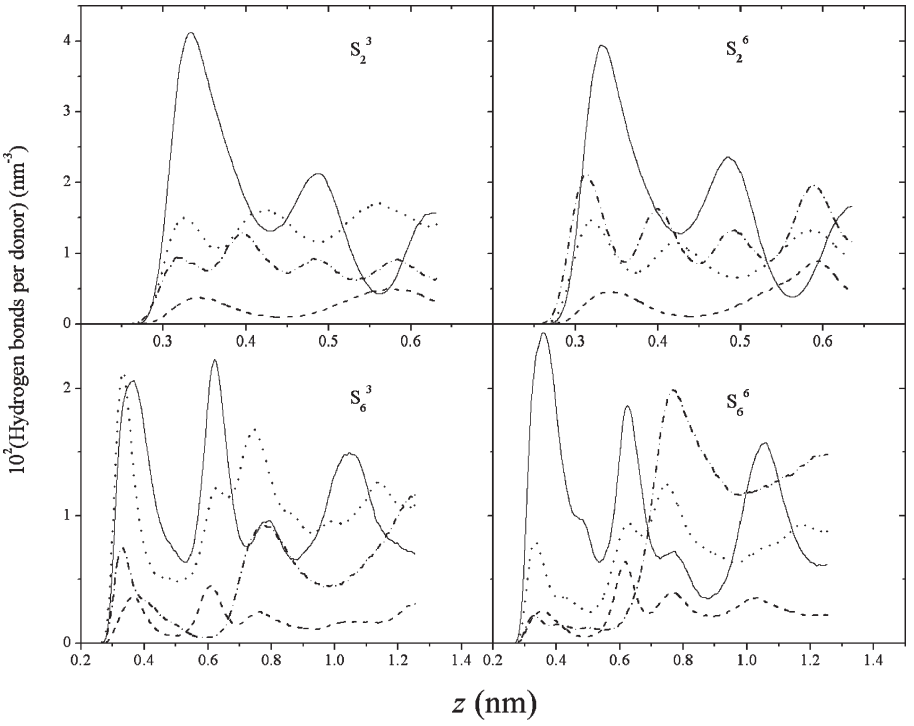

Figure 8. Hydrogen bond density profiles for N−H···O_A (solid curve), N−H···O_W (dashed curve), O−H···O_A (dotted curve), and O−H···O_W (dashed-dotted curve).

respectively, depending on the degree of confinement and on the organization of polymer layers beside the surfaces. Even in the bulk samples, around half of the amide groups are not accessible to the water molecules, meaning that additional water molecules accumulate into clusters. This is consistent with the critical concentration of 3−4 wt % water obtained in positron annihilation lifetime spectroscopy[77,78] and dynamical mechanical analysis[13] for the transitions in free volume behavior or decrease of the main relaxation temperature of bulk PA-6,6; should all amide group be available to water molecules, the critical water concentration would be 7 wt %.

The number of O−H···O_W hydrogen bonds also depends on the water content of polymer and on the intersurface distance. Increasing the distance between the confining surfaces increases the number of O−H···O_W hydrogen bonds. The amount of increase again depends on the layering behavior of water molecules; in the case of highly confined systems, S_1^3 and S_1^6, due to the geometrical restrictions the number of O−H···O_W hydrogen bonds are low. The maximum number of O−H···O_W hydrogen bonds for a polymer sample containing 3 wt % water is observed in system S_5^3, in which well-organized layers are formed between the surfaces, and the surfaces are far away enough not to impose strong geometrical restrictions.

Hydrogen Bond Profiles. To have a better picture of hydrogen bonding in nanoconfined PA-6,6+water systems, in Figure 8 the hydrogen bond (per donor) profiles for N−H···O_A, N−H···O_W, O−H···O_A, and O−H···O_W bonds are shown for wet polymer systems S_2 and S_6, as typical examples. According to the results in Figure 8, the hydrogen bond profiles show oscillatory behavior because of the layering of both polymer and water in the confined region. The results show that the N−H···O_A constitutes the majority of hydrogen bonds in the wet polymer sample. A comparison of the distribution functions in Figure 2 and the profiles in Figure 8 show that at small intersurface separations the majority of hydrogen bonds between amide groups and water molecules are formed within the layers. With increasing distance between the surfaces, the hydrogen bonds are formed both within and between the layers. This is in complete agreement with the results of our previous work on the hydrogen bonding of nanoconfined PA-6,6.[55]

An examination of the hydrogen bond density profiles in Figure 8 reveal a correlation between the N−H···O_A, O−H···O_A, and N−H···O_W hydrogen bond profiles. In narrow pores, where the N−H···O_A hydrogen bonds are mainly formed inside the layers, the positions of the maxima in these profiles correspond to each other. However, there are extra peaks in the O−H···O_A and N−H···O_W hydrogen bond profiles, belonging to hydrogen bonding among water molecules, located between the polymer layers, and their neighboring polymer layers. In narrow pores, very few N−H···O_A bonds are formed between the polymer layers; therefore, such maxima in the O−H···O_A and N−H···O_W hydrogen bond profiles correspond to the minima in the N−H···O_A profiles. In wide pores, on the other hand, N−H···O_A hydrogen bonds can be formed between the layers as well as inside the layers (see Figure 8, bottom panel). In such pores, the positions of maxima in N−H···O_A, O−H···O_A, and N−H···O_W hydrogen bond profiles roughly correspond to each other. These findings indicate that water molecules can penetrate (dissolve) in the polymer layers close to the surfaces to form hydrogen bonds with amide groups. Moreover, they can locate between the polymer layers and act as a bridge between the polymer layers by forming hydrogen bonds with their neighboring amide groups. In other words, the origin of water solubility in nanoconfined PA-6,6 is the ability of organization of water and polymer layers in such a way to form hydrogen bonds.

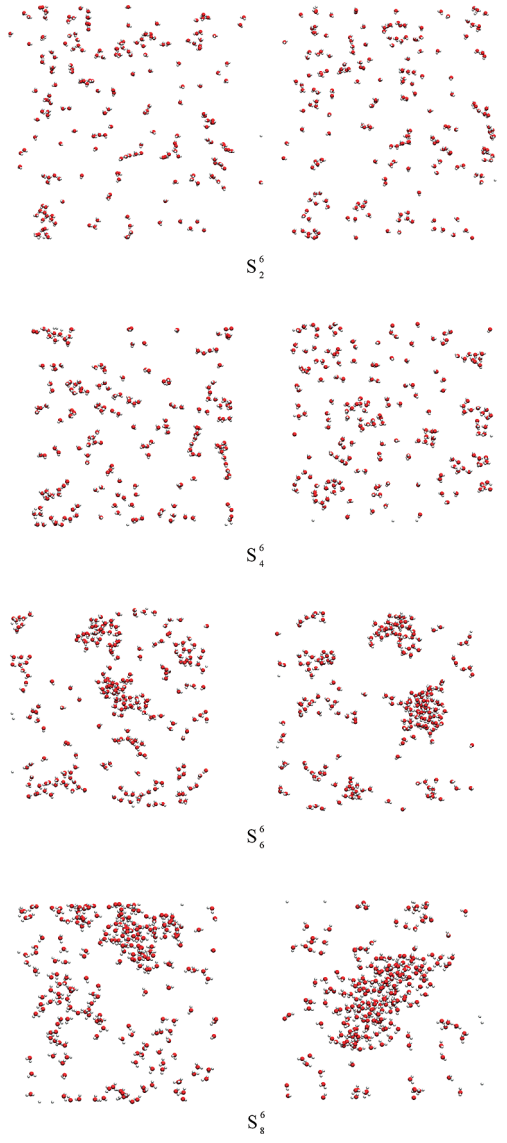

Figure 9. Snapshots of the simulation box. The left and right pictures represent the snapshots at 10 and 50 ns, respectively. For clarity, the polymer molecules and the surfaces are removed and only water molecules are shown.

A close look at the hydrogen bond profiles for systems containing 3 and 6 wt % water in Figure 8 shows that increasing the water content, O−H···O_A and O−H···O_A hydrogen bond density profiles in small pores (see Figure 8 top panel) obey similar trends. This indicates that the added water molecules distribute in the whole box volume. Addition of water molecules to the polymer matrix in larger pores (see Figure 8 bottom panel) causes the hydrogen bonding between water molecules and between water−polymer molecules to be mainly extended to the central region of the box. This might be indicative of a phase-separated system in large pores. In the following section we discuss the possibility of such a phase transition.

Water Clustering. As stated before, sharp peaks in the surface-water distribution functions in Figure 2 and the O−H···O_A hydrogen bond profiles in Figure 8, for mixtures containing 6 wt % water, might be an indication of water clustering or even phase separation in PA-6,6+water system. We have shown in Figure 9

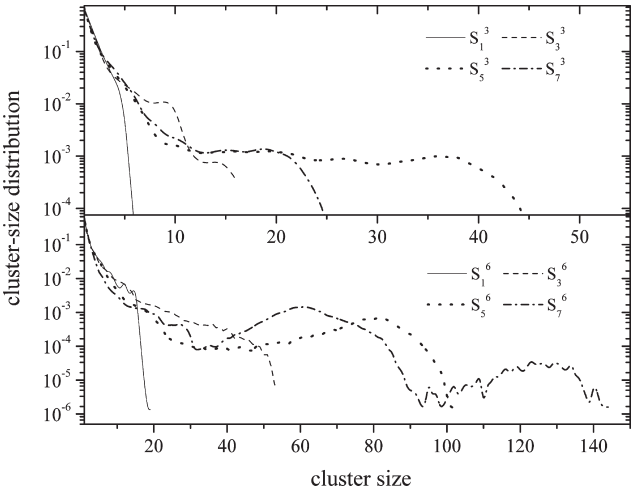

Figure 10. Normalized distribution functions for clusters of water molecules as functions of cluster sizes. The clusters are calculated within a sphere of 0.3 nm radius.

snapshots of simulation boxes for different systems. For the sake of clarity, the surfaces and the polymer molecules are removed from the snapshots, and only the water molecules are shown in Figure 9. The results in Figure 9 indicate the formation of big and stable water clusters, especially with increasing the separation distance between the surfaces.

To quantify the water clustering in a nanoconfined PA-6,6 +water system, we have considered those water molecules forming spherical aggregates with a density higher than a critical value as water clusters. In fact, for each water molecule, a list of neighboring molecules, sorted in order of increasing O_W−O_W distance, is formed. Any neighbor within a distance of 0.3 nm from a fixed oxygen atom is regarded as a connected atom and belonging to the same cluster. When more than three molecules belong to the same cluster, a further requirement to consider additional molecules in the cluster is that the mass density must remain above a critical value of 900 kg m^{-3}. To calculate the density, the mass of clustered water molecules is divided by the volume of a sphere centered at the center of mass of the cluster.

We have shown in Figure 10 the normalized distribution of cluster sizes for some confined systems containing 3 and 6 wt % water. The results show that at lower water concentrations no big clusters are formed. At higher water concentrations, relatively small clusters are formed in the narrower pores, but increasing the pore width allows the formation of bigger clusters. In system S_7^6, with a surface separation of about 4.0 nm, very big clusters are formed in the center of the pore (see Figure 2 for comparison). Even bigger clusters are formed in the bulk sample (not shown here). These findings indicate that geometrical confinement does not allow the formation of big water clusters in the PA-66+water confined systems. Instead, as shown in the preceding section, the PA−water hydrogen bonding distributes water molecules all over the whole box volume. In fact the formation of hydrogen bonds between water molecules, in large pores, stables such clusters. Since in highly confined geometries the number of hydrogen bonds between water molecules is much less than those of the bulk fluid, the formation of bigger clusters is precluded in such systems.

To be able to more quantitatively understand the effect of water clustering in the system, we have shown in Figure 11 the

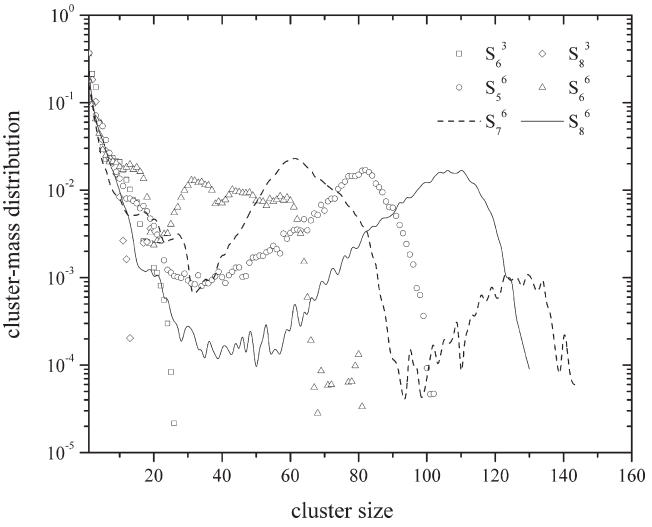

Figure 11. Normalized distribution functions for mass of clusters versus the cluster sizes.

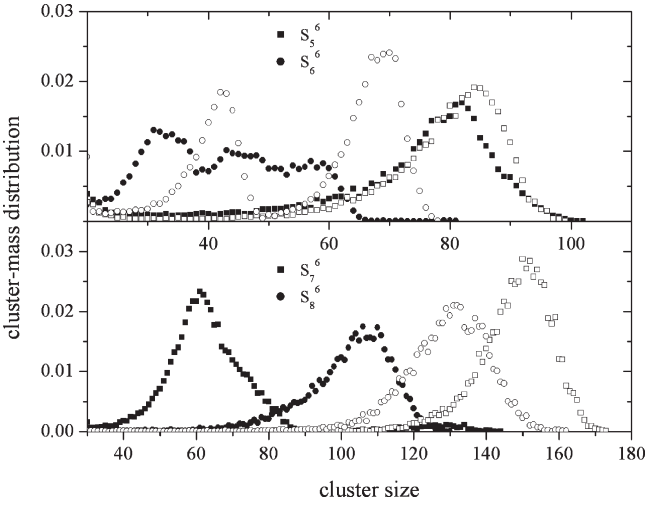

Figure 12. Distribution functions for cluster masses. The filled and the corresponding open markers represent the distribution functions at 10 and 50 ns, respectively. Note that here just the growth of bigger clusters with time are shown.

normalized distribution functions for cluster masses as a function of cluster sizes. The results show that in systems containing 6 wt % water and with a relatively large intersurface separation (>2 nm) big clusters are formed in the center of box. Our analysis show that formation of such big clusters is an indication of phase separation in PA-6,6+water system. The phase separation is, however, a very slow process which cannot be observed directly in a few nanoseconds of simulation. To further validate the possibility of phase separation in PA-6,6+water systems in the present study, we have performed very long simulations, over a 50 ns time span, to see whether the clusters are changing their sizes with the passage of time or not. In Figure 12 we have shown the normalized cluster-mass distributions for systems S_5^6-S_8^6 as typical examples, after 10 and 50 ns of simulation. For the sake of clarity, just a part of the normalized distribution functions involving bigger size clusters are shown in Figure 12. The results reveal that the mass distribution of big clusters shows more intense peaks with the passage of time. Moreover, their maximum distribution shift to bigger cluster sizes, indicating the growth of big clusters in the system. For systems nanoconfined in smaller pores, however, the cluster growth was not observed in 50 ns. We have also shown in Figure 9 snapshots of the simulation box after 50 ns of simulation, for comparison. Visual observation of the snapshots in Figure 9 also indicates the growth of water clusters in bigger pores.

The results in the present and preceding sections show that nanoconfinement of PA-6,6+water in small size pores increases the water solubility. Such an increase in the water solubility is the result of forcing water molecules, by the surfaces, into the polymer layers. Since the confined polymer molecules can not adequately form hydrogen bonds with each other, due to the geometrical restrictions, water molecules inside the polymer have more freedom to adopt such a configuration to form strong hydrogen bonded structures with the amide groups. Part of the water molecules present between the polymer layers can also adequately form hydrogen bonds with their neighboring polymer layers. With increasing the pore size, on the other hand, polymer molecules can better form hydrogen bonds among each other and amide groups become less available to water molecules. Consequently, the water molecules start clustering together, due to the hydrogen bonds. These clusters can grow with time, a process which finally leads to the phase separation in big pores (and in bulk).

CONCLUSIONS

A new MD simulation scheme,[58] developed for simulation of fluids in confined geometries, is employed to simulate PA-6,6 +water nanoconfined between graphene monolayers. The simulation method is shown to simulate the fluid in the confinement in equilibrium with the bulk fluid. Here, three types of systems; dry polymer, polymer+3 wt % water, and polymer+6 wt % water, were studied. To be able to study the effect of confinement degree (at a fixed composition) on the structural properties of polymer a number of systems at different intersurface separations, and hence different layering capabilities, have been studied. Bulk samples of polymer+water were also prepared, in order to be able to compare the properties of nanoconfined systems with those of the bulk.

The results of the present study show that both water and polymer molecules form organized layers near the surfaces. As usual, well-organized layers lead to strong positive solvation forces, while the formation of diffuse layers corresponds to negative solvation forces. It is shown that the polymer swells in the presence of water and stretches parallel to the surfaces. The swelling depends on the confinement and increases with the pore size. The study of hydrogen bonding in polymer−water system show that around 10−15% of the N−H···O_A hydrogen bonds break with the addition of 3 wt % water to the polymer. Addition of more water molecules to the system (up to 6 wt %) breaks only very few additional N−H···O_A hydrogen bonds. This is in agreement with the dynamical mechanical analysis results of Le Huy and Rault[13] on PA samples at 300 K and with the previous reports in the literature on bulk polymers.[19,73−76]

It is further indicated that in narrow pores, due to the geometrical restrictions in the confined region, the bigger PA molecules can not arrange in such way to form hydrogen bonds corresponding to the bulk polymer. On the other hand, the surfaces force the water molecules in polymer layers and hydrogen bonding between amide−water can well stabilize such a

dx.doi.org/10.1021/jp204423z |J. Phys. Chem. B 2011, 115, 9720–9731

system. Addition of water molecules to PA-6,6+water system, confined in wide pores, accumulates water molecules into clusters. In such wide pores, the amide groups are not as accessible to water molecules, therefore hydrogen bonding between the water−polymer cannot stabilize the mixture. The hydrogen bonding between water molecules therefore acts as a driving force for the formation of big water clusters. These findings are in agreement with the critical concentration of 3−4 wt % water obtained in positron annihilation lifetime spectroscopy[77,78] and dynamical mechanical analysis experiments.[13] Our analysis shows that such big clusters grow with the passage of time and phase-separate from the mixture. Considering the fact that solubility of sorbants in a shorter chain polymer is lower than in the longer chain ones,[72] the phase-separation of PA-6,6 + 6 wt % water system in bulk is in agreement with our recent grand canonical ensemble simulation results[71] and with experimental solubility data.[79−81] Nanoconfinement in small pores, however, is shown to increase the water solubility of the polymer. Such a result is in agreement with previous experimental findings on liquid−liquid phase equilibria in nitrobenzene+n-hexane mixtures in bulk and in pores.[82]

AUTHOR INFORMATION

Corresponding Author

*E-mail: h.eslami@theo.chemie.tu-darmstadt.de.

ACKNOWLEDGMENT

H.E. gratefully acknowledges the computer facilities provided by the research committee of Persian Gulf University. Partial support of this work by Alexander von Humboldt Foundation is highly acknowledged.

REFERENCES

(1) Chauveteau, G.; Tirrell, M.; Omari, A. *J. Colloid Interface Sci.* **1984**, *100*, 41.
(2) Allen, R. C.; Budowle, B. *Gel Electrophoresis of Proteins and Nucleic Acids: Selected Techniques*: de Gruyter: Berlin, 1994.
(3) Yau, W. W.; Kirkland, J. J.; Bly, D. D. *Size-Exclusion Liquid Chromatography*; Winefordner, J. D., Ed.; John Wiley: New York, 1989; Vol. 98, pp 277−316.
(4) Zakin, J. L.; Hunston, D. L. J. *Macromol. Sci. Phys.* **1980**, *B18*, 795.
(5) Block, H. *Molecular Behavior and the Development of Polymeric Materials*; Ledwith, A., North, A. M., Eds.; Chapman & Hall: London, 1975.
(6) Peng, X.; Jin, J.; Nakamura, Y.; Ohno, T.; Ichinose, I. *Nat. Nanotechnol.* **2009**, *4*, 353.
(7) Vrij, A. *Pure Appl. Chem.* **1976**, *48*, 471.
(8) Naper, D. H. *Polymeric Stabilization of Colloidal Dispersions*; Academic: London, 1983.
(9) Lal, M.; Watson, G. M. *ACS Symp. Ser.* **1984**, *240*, 205.
(10) Kohn, M. *Nylon Plastics Handbook*; Hanser-Gardner Publications: New York, 1995.
(11) Sridhar, S.; Smitha, B.; Mayor, S.; Prathab, B.; Aminabhavi, T. M. *J. Mater. Sci.* **2007**, *42*, 9392.
(12) Mai, Y. W.; Williams, J. G. *J. Mater. Sci.* **1977**, *12*, 1376.
(13) Le Huy, H. M.; Rault, J. *Polymer* **1994**, *35*, 136.
(14) Skrovanek, D. J.; Howe, S. E.; Painter, P. C.; Coleman, M. M. *Macromolecules* **1985**, *18*, 1676.
(15) Miura, H.; Hirschinger, J.; English, A. D. *Macromolecules* **1990**, *23*, 2153.
(16) Jones, N. A.; Atkins, E. D. T.; Hill, M. T.; Cooper, J. S.; Franco, L. *Macromolecules* **1997**, *30*, 3569.
(17) Murthy, N. S.; Wang, Z. G.; Hsiao, B. S. *Macromolecules* **1999**, *32*, 5594.
(18) Murthy, N. S. *J. Polym. Sci.: Polym. Phys.* **2006**, *44*, 1763.
(19) Goudeau, S.; Charlot, M.; Vergelati, C.; Müller-Plathe, F. *Macromolecules* **2004**, *37*, 8072.
(20) Karimi-Varzaneh, H. A.; Carbone, P.; Müller-Plathe, F. *Macromolecules* **2008**, *41*, 7211.
(21) Bhushan, B.; Israelachvili, J. N.; Landman, U. *Nature (London)* **1995**, *374*, 607.
(22) Israelachvili, J. N.; McGuiggan, P. M.; Homola, A. M. *Science* **1988**, *240*, 189.
(23) Zhu, L.; Cheng, S. Z. D.; Huang, P.; Ge, Q.; Quirk, R. P.; Thomas, E. L.; Lotz, B.; Hsiao, B. S.; Yeh, F.; Liu, L. *Adv. Mater.* **2002**, *14*, 31.
(24) Sun, L.; Zhu, L.; Ge, Q.; Quirk, R. P.; Xue, C.; Cheng, S. Z. D.; Hsiao, B. S.; Avila-Orta, C. A.; Sics, I.; Cantino, M. E. *Polymer* **2004**, *45*, 2931.
(25) Ellison, C. J.; Mundra, M. K.; Torkelson, J. M. *Macromolecules* **2005**, *38*, 1767.
(26) Bureau, L. *Rev. Sci. Instrum.* **2007**, *78*, 065110.
(27) Yousfi, M.; Porcar, L.; Lindner, P.; Boue', F.; Rharbi, Y. *Macromolecules* **2009**, *42*, 2190.
(28) Baber, S.; Zhou, M.; Lin, Q. L.; Naalla, M.; Jia, Q. X.; Lu, Y.; Luo, H. M. *Nanotechnology* **2010**, *21*, 165603.
(29) Kim, S.; Mundra, M. K.; Roth, C. B.; Torkelson, J. M. *Macromolecules* **2010**, *43*, 5158.
(30) Snook, I. K.; Van Megan, W. *J. Chem. Phys.* **1980**, *72*, 2907.
(31) Cleveland, C. L.; Landman, U.; Bamett, R. N. *Phys. Rev. Lett.* **1982**, *49*, 790.
(32) Magda, J. J.; Tirrell, M.; Davis, H. T. *J. Chem. Phys.* **1985**, *83*, 1888.
(33) Schoen, M.; Rhykerd, C. L.; Diestler, D. J.; Cushman, J. H. *Science* **1989**, *245*, 1223.
(34) Bitsanis, J.; Somars, S. A.; Davis, H. T.; Tirrell, M. *J. Chem. Phys.* **1990**, *93*, 3427.
(35) Schoen, M.; Diestler, D. J.; Cushman, J. H. *J. Chem. Phys.* **1994**, *100*, 7707.
(36) Todd, B. D.; Evans, D. J.; Daivis, P. J. *Phys. Rev. E* **1995**, *52*, 1627.
(37) Gao, J.; Luedtke, W. D.; Landman, U. *Phys. Rev. Lett.* **1997**, *79*, 705.
(38) Wang, J. C.; Fichthorn, K. A. *J. Chem. Phys.* **2000**, *112*, 8252.
(39) Mansfield, K. F.; Theodorou, D. N. *Macromolecules* **1989**, *22*, 3143.
(40) Yethiraj, A.; Hall, C. K. *Macromolecules* **1990**, *23*, 1865.
(41) Bitsanis, I. A.; Pan, C. *J. Chem. Phys.* **1993**, *99*, 5520.
(42) Yethiraj, A. *J. Chem. Phys.* **1994**, *101*, 2489.
(43) Ballamudi, R. K.; Bitsanis, I. A. *J. Chem. Phys.* **1996**, *105*, 7774.
(44) Gao, J.; Luedtke, W. D.; Landman, U. *J. Phys. Chem. B* **1997**, *101*, 4023.
(45) Aoyagi, T.; Takimoto, J.; Doi, M. *J. Chem. Phys.* **2001**, *115*, 552.
(46) Cui, S. T.; Cummings, P. T.; Cochran, H. D. *J. Chem. Phys.* **2001**, *114*, 7189.
(47) Jeon, J. H.; Kim, S. H.; Jo, W. H. *Macromol. Theory Simul.* **2002**, *11*, 147.
(48) Cui, S. T.; McCabe, C.; Cummings, P. T. *J. Chem. Phys.* **2003**, *118*, 8941.
(49) Choudhury, N.; Pettitt, B. M. *J. Am. Chem. Soc.* **2005**, *127*, 3556.
(50) Leng, Y.; Cummings, P. T. *Phys. Rev. Lett.* **2005**, *94*, 026101.
(51) Marti, J.; Nagy, G.; Gordillo, M. C.; Guardia, E. *J. Chem. Phys.* **2006**, *124*, 094703.
(52) Borodin, O.; Smith, G. D.; Bandyopadhyaya, R.; Byutner, O. *Macromolecules* **2003**, *36*, 7873.
(53) Daoulas, K. Ch.; Harmandaris, V. A.; Mavrantzas, V. G. *Macromolecules* **2005**, *38*, 5780.
(54) Harmandaris, V. A.; Daoulas, K. Ch.; Mavrantzas, V. G. *Macromolecules* **2005**, *38*, 5796.
(55) Eslami, H.; Müller-Plathe, F. *J. Phys. Chem. B* **2009**, *113*, 5568.

(56) Eslami, H.; Müller-Plathe, F. *J. Phys. Chem. B* **2010**, *114*, 387.
(57) Wang, Y.; Hill, K.; Harris, J. G. *J. Chem. Phys.* **1993**, *100*, 3276.
(58) Eslami, H.; Mozaffari, F.; Moghadasi, J.; Müller-Plathe, F. *J. Chem. Phys.* **2008**, *129*, 94702.
(59) Schoen, M.; Diestler, D. J.; Cushman, J. H. *J. Chem. Phys.* **1987**, *87*, 5464.
(60) Schoen, M.; Diestler, D. J.; Cushman, J. H. *J. Chem. Phys.* **1994**, *100*, 7707.
(61) Schoen, M.; Diestler, D. J.; Cushman, J. H. *Phys. Rev. B* **1993**, *47*, 5603.
(62) Berendsen, H. J. C.; Postma, J. P. M.; van Gunsteren, W. F.; DiNola, A.; Haak, J. R. *J. Chem. Phys.* **1984**, *81*, 3684.
(63) Müller-Plathe, F. *Comput. Phys. Commun.* **1993**, *78*, 77.
(64) Tarmyshov, K.; Müller-Plathe, F. *J. Chem. Inf. Model.* **2005**, *45*, 1943.
(65) Berendsen, H. J. C.; Grigera, J. R.; Straatsma, T. P. *J. Phys. Chem.* **1987**, *91*, 6269.
(66) Allen, M. P.; Tildesley, D. J. *Computer Simulation of Liquids*; Clarendon Press: Oxford, 1987.
(67) Goudeau, S.; Charlot, M.; Müller-Plathe, F. *J. Phys. Chem. B* **2004**, *108*, 18779.
(68) Eslami, H.; Dargahi, A.; Behnejad, H. *Chem. Phys. Lett.* **2009**, *473*, 66.
(69) Ryckaert, J. P.; Ciccotti, G.; Berendsen, H. J. C. *J. Comput. Phys.* **1997**, *23*, 327.
(70) Müller-Plathe, F.; Brown, D. *Comput. Phys. Commun.* **1991**, *64*, 7.
(71) Eslami, H.; Mehdipour, N. *Phys. Chem. Chem. Phys.* **2011**, *14*, 669.
(72) Cuthbert, T. R.; Wagner, N. J.; Paulaitis, M. E. *Macromolecules* **1997**, *30*, 3058.
(73) Starkweather, H *J. Appl. Polym. Sci.* **1959**, *11*, 129.
(74) Müller-Plathe, F. *J. Chem. Phys.* **1998**, *108*, 8252–8263.
(75) Borodin, O.; Bedrov, D.; Smith, G. D. *J. Phys. Chem. B* **2002**, *106*, 5194.
(76) Smith, G. D.; Bedrov, D.; Borodin, O. *Phys. Rev. Lett.* **2000**, *85*, 5583.
(77) Dlubek, G.; Stolp, M.; Nagel, C.; Fretwell, H. M.; Alam, M. A.; Radusch, H. J. *J. Phys.: Condens. Matter* **1998**, *10*, 10443.
(78) Dlubek, G.; Redmann, F.; Krause-Rehberg, R. *J. Appl. Polym. Sci.* **2002**, *84*, 244.
(79) Lim, L.; Britt, I. J.; Tung, M. A. *J. Appl. Polym. Sci.* **1999**, *71*, 197.
(80) Watt, I. C. *J. Macromol. Sci. A: Pure Appl. Chem.* **1980**, *14*, 245.
(81) Schaffer, M. A.; Mcauley, K. B.; Cunningham, M. F. *Polym. Eng. Sci.* **2003**, *43*, 639.
(82) Gelb, L. D.; Gubbins, K. E.; Radhakrishnan, R.; Sliwinska-Bartkowiak, M. *Rep. Prog. Phys.* **1999**, *62*, 1573.